# Enhance P wave imaging using elastic dynamic matching FWI

## Introduction

Full waveform inversion (FWI) has been developed such that it can be routinely applied to derive accurate velocity models with high resolution, from which a synthetic dataset can best match with the recorded one. The derived models can serve as input for depth migration or be used directly to derive a least squares equivalent image called FWI Image (Wang, et. al., 2021). Up to now, FWI has been mostly applied in acoustic media, where acoustic wave equations are employed to synthesize the data and compute the gradient. Thanks to the steady progress in computing power as well as seismic data quality such as acquisition of ocean bottom node data, the interest in accounting for the elasticity by applying elastic FWI has considerably increased for model building (Wang, et. al., 2021). Many elastic FWI algorithms utilize the elastic wave equation for wavefield propagation while focusing on inverting the P wave velocity ($v_p$), other elastic parameters, like shear wave velocity ($v_s$) and density ($\rho$), are computed following some empirical relations with certain constraints (Raknes, et. al., 2015).

In this paper, we propose an elastic dynamic matching FWI (EDMFWI) as an extension of the acoustic algorithm. With the successful applications to variety of datasets, it demonstrates the significance to improve P-wave imaging in different scenarios: in a shallow ocean bottom cable (OBC) acquisition in North Sea, EDMFWI successfully inverts the velocity for a target reservoir with a known class 2p amplitude variation with offset response; its application to a sparse OBN data in deep water Gulf of Mexico produces a velocity model with better focused salt boundary and reduced salt halo resulting improved image underneath; the final example is from a DAS-VSP survey also in deep water, Gulf of Mexico, where elastic FWI takes advantage of the contribution from mode converted wave at salt interfaces benefiting considerably subsalt images.

## Elastic Dynamic Matching FWI

Elastic FWI solves the elastic wave equation on staggered grid using high order finite differences with optimized coefficients:

$$\begin{cases} \rho \dfrac{\partial v_i}{\partial t} = \tau_{ij,j} + \mathbf{f_s} \\ \dfrac{\partial \tau_{ij}}{\partial t} = c_{ijkl} v_{k,l} \end{cases} \tag{1}$$

Here $v_i$ is the particle velocity for component $i$, $\tau_{ij}$ are the components of the stress tensor, $c_{ijkl}$ are the elastic moduli, here $(i, j, k, l = 1,2,3)$ represents the different component. $\rho$ is the density, and $\mathbf{f_s}$ is a source term.

The proposed EDMFWI uses the similar objective function as the acoustic algorithm, which maximizes the windowed cross-correlation of the recorded and synthetic data after their dynamic matching (Mao, et. al., 2020):

$$E = \int_{x_s} \int_{x_r} \int_{t} \int_{x_r - x_0}^{x_r + x_0} \int_{t-\tau_0}^{t+\tau_0} w(x,\tau)\hat{d}(x,\tau,X)\bar{u}(x,\tau,X)\, d\tau dx\, dt dx_r dx_s, \tag{2}$$

where $X = (x_r, x_s)$ with $x_r, x_s$ being the receiver and source coordinate, respectively. $w(x,\tau)$ is a weighting function. To better honour the amplitude of the field data, EDMFWI uses an optimized dynamic matching scheme in conditioning the recorded data $(d)$ and the synthetic one $(u)$; $x_0$ and $\tau_0$ is the local half window length, respectively.

Even though elastic FWI can be applied to invert multiple elastic parameters like $v_p, v_s$ and density$(\rho)$ together, it has been a widely adopted approach to concentrate on inverting P wave property only. This is partially because P wave properties are the dominant component of signal mostly used in seismic exploration.

The P wavefield in the elastic system of wave equations in Equation (1) can be formulated to explicitly relate it to the shear properties of the earth as follows,

$$\frac{\partial^2}{\partial t^2}P = \alpha\nabla^2 P + P\nabla^2(\alpha - 2\beta) + 2\nabla\alpha\cdot\nabla P - 2\nabla\beta\cdot(\nabla\times \mathrm{S}) + \frac{1}{\rho}[P\nabla(\alpha-2\beta) + \alpha\nabla P - \beta(\nabla\times \mathrm{S})]\cdot\nabla\rho + \frac{\alpha-2\beta}{\rho}P\left(\nabla^2\rho - \frac{1}{\rho}\nabla\rho\cdot\nabla\rho\right) \quad (3)$$

Where $P = \nabla\cdot V$ and $\vec{S} = \nabla\times V$ , $V = (v_1, v_2, v_3)$, $\alpha = v_p^2$ and $\beta = v_s^2$ with $v_p, v_s$ being the p and s wave velocity, respectively. If density is constant, equation (3) reduces to the one in Li, et. al. (2018).

Equation (3) shows the explicit dependency of P wave propagation to the gradient of shear wave velocity. Thus, elastic FWI is expected to have a significant impact on P wave velocity at a strong subsurface interface like the boundaries of salt or basalt.

Elastic wave equation can simulate seismic data with the correct amplitude and phase variation with offset or angle which acoustic wave equation is incapable of handling. This can be extremely important for accurate inversion of model properties associated with a hydrocarbon reservoir because variations in amplitude and phase often present in such cases.

**Examples**

**Case 1:** The first example is an OBC dataset from a shallow water environment in the North Sea. At the reservoir, there is an opposite trend between $v_p, v_s$ and density ($\rho$) (Figure 1a). A prestack CMP gather (Figure 1b) nearby the displayed well exhibits a polarity reversal as offset increases. With the model parameters decoded from the well logs, analytical reflection coefficient shows a class 2p AVO anomaly as shown in Figure 1c). The 1D elastic modelling confirms the phase reversal as offset increases (Figure 1d); as expected, the acoustic modelling result can not simulate this variation (Figure 1e).

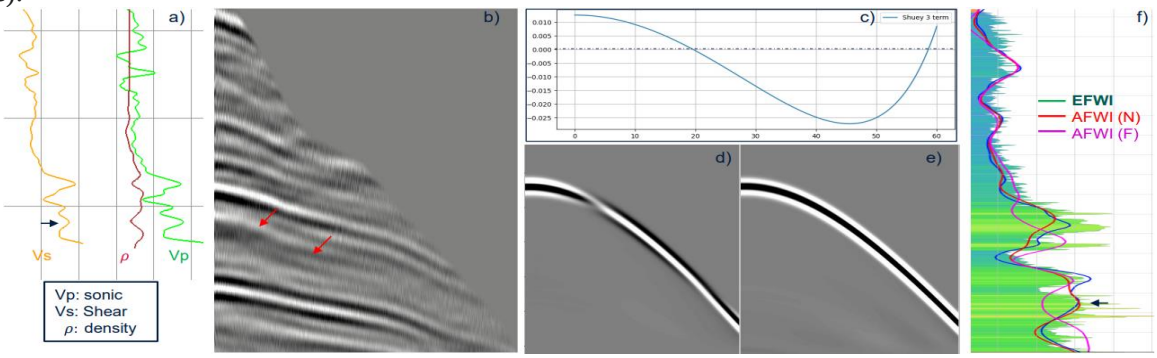


Figure 1: a) Three well logs; b) a CMP gather close to the reservoir showing amplitude and phase polarity reversal while increasing offset; c) Reflection coefficient computed using Shuey's equation; elastic(d) and acoustic (e) synthetic data of the 1D model; f) three FWI inverted velocities overlaid with the sonic log. The arrow shows the depth resulting in a class 2p AVO curve.

EDMFWI was applied to this dataset where only $v_p$ is inverted, $v_s$ and $\rho$ are computed following some analytical equations constrained with wells. It produces a high-resolution velocity with the properly recovered anomaly (green line in Figure 1f). Figure 2a) shows a section of the inverted $v_p$ model. Figure 2b) is the corresponding FWI image. Although acoustic FWI(AFWI) predicts the kinematics of the arrivals, the phase reversal at the reservoir depth challenges the acoustic algorithm. To overcome the acoustic limitations, the input data was split to near and far angle corridors, and acoustic FWI was applied to each separately (Gao, et. al., 2023). Figures 2c and 2e shows the acoustic FWI results for the near- and far-angle data, respectively, and Figures 2d and 2f are the corresponding FWI image. Contrasting the results, EDMFWI recovers the velocity features shown in far angle AFWI result as marked in the figure and also the velocity anomaly shown in the near angle acoustic inversion, but missed in the far angle AFWI result. Among the three velocities shown in Figure 1f), EDMFWI result has the best match with the sonic log. The near angle AFWI result also matches the sonic log around the target area, but it has much lower resolution due to limited data are used in the inversion, while the far angle result of acoustic propagation shows an opposite trend, namely, velocity decreasing rather than increasing as it does not honour the elastic behaviour.

**Case 2:** The second example is a sparse node dataset from the Gulf of Mexico with ultralong offset of

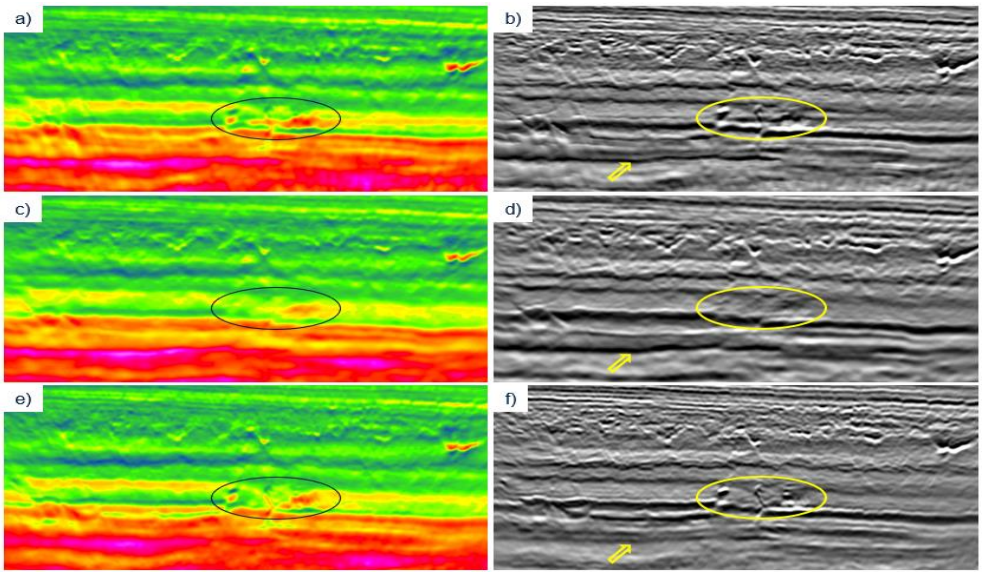


Figure 2: a) P wave velocity after 25 Hz elastic FWI; b) FWI image from the velocity in a); c) Acoustic FWI velocity using near angle data; d) FWI image from the velocity in c); e) Acoustic FWI velocity using far angle data and f) FWI image for the velocity in e).

45 km. The area contains extensive shallow salt bodies. Both acoustic and elastic FWI were run to a maximum frequency of 12 Hz. As shown in Equation 3, p-wavefield is more sensitive to elastic effects at large shear velocity contrasts. Compared to the acoustic FWI result (Figure 3a), elastic DMFWI produces a velocity model with a sharper salt interface and significantly reduced salt halo (Figure 3b). The resulting FWI images (Figures 3c and 3d) show improved focusing and better continuity in the subsalt area for elastic FWI model. Figures 3e and 3f compares a depth slice of the acoustic RTM images using the inverted velocities, respectively. Clearly it is observed that elastic FWI results in better focusing at the salt boundary as pointed by the arrow.

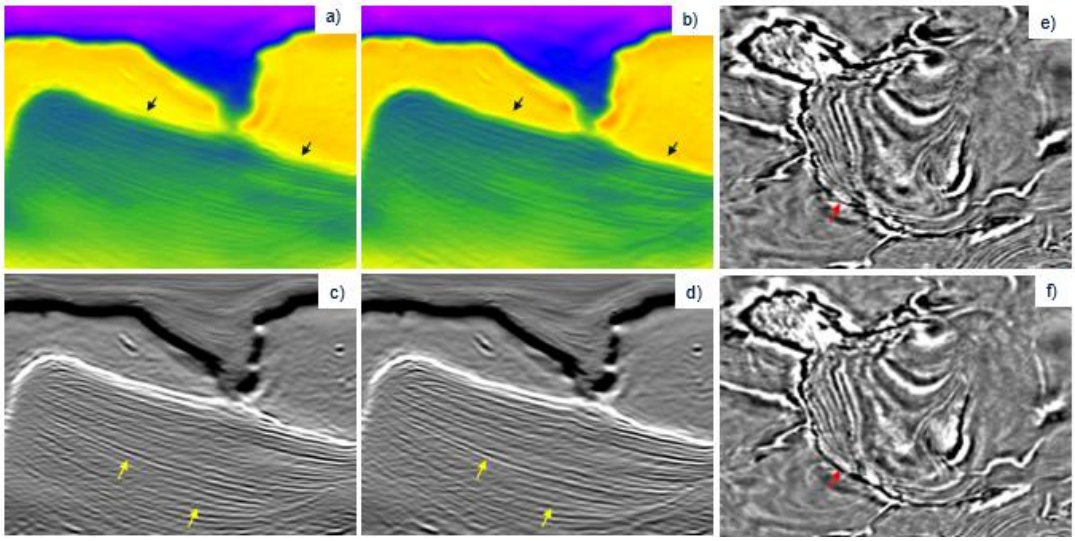


Figure 3: a) Acoustic FWI velocity and image in (c); b) velocity after elastic FWI and FWI image (d); e) is the depth slice of RTM using acoustic FWI model compared to that using elastic FWI model (f).

**Case 3:** The 3rd dataset is from a DAS-VSP survey in the Gulf of Mexico as well. The specific acquisition poses a unique challenge for acoustic FWI. A double converted P-wave at the salt interface (P to S at top salt and back to P at the base) is missing from the snapshot of acoustic propagation (Figures 4a) which is clearly presented in the elastic wavefield (Figures 4b). With elastic FWI, such locally mode converted wave can improve the illumination of measured P data. Properly utilizing this event is particularly important for DAS-VSP data due to the very limited fold coverage associated with this type of acquisition, thus adding to the list of advantages of elastic over acoustic FWI. Compared to the

acoustic FWI image in Figure 4c, the FWI image from elastic FWI (Figure 4d) is better focused with improved event continuity and less artefact.

## Conclusions

By employing the elastic wave equation for wavefield propagation, elastic dynamic matching FWI produces an accurate velocity model that better represents the earth's geology under consideration. It properly simulates the variation of reflection amplitude and phase with offset associated with a reservoir. FWI images derived from elastic FWI have better resolution than those produced from acoustic FWI. Improved sediment-salt boundaries and reduced salt halos allow better images of the subsalt. In addition, taking advantage of the mode converted energy at salt interfaces enhances the subsalt images for DAS-VSP data alleviating the limited fold coverage due to the specific acquisition geometry.

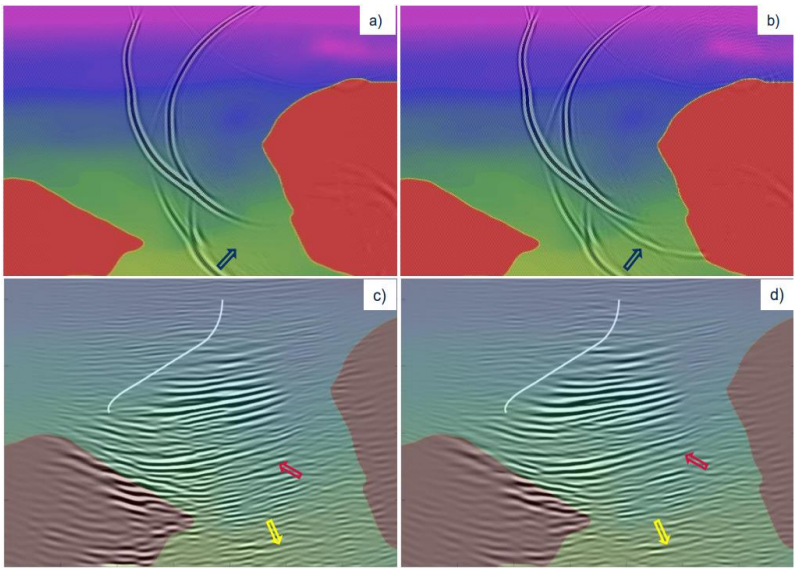


Figure 4: a) snapshot associated with acoustic FWI; b) the same snapshot associated with elastic FWI, the blue arrow points to a mode converted wave at salt boundary (PSP); c) 25 Hz acoustic FWI image overlaid with velocity model and d) 25 Hz elastic FWI image overlaid with velocity model.

## Acknowledgements

We thank TGS management team, Josef Heim, Paul Farmer and Adriana Citlali Ramirez, for their support and permission to publish this work, and sincerely appreciate Yuriy Ivanov from Aker Bp for all his kind help and detailed comments to the paper. Finally we thank Aker BP and Vår Energi ASA for allowing us to use the North Sea data, Shell and BP Exploration and Production Inc. for the DAS example and TGS Multiclient for the sparse node data.

## References

Gao, F., Dong, S., He, Y., Sheng, J., Liu, F., Wang, B., Calderon, C., Ivanov, Y., Marcy, F.D. and Aaker, O.E. [2023], High resolution imaging by dynamic matching FWI in the presence of AVO effects, Extended Abstract, SEG 93rd Annual meeting

Li, Y. E., Du, Y., Yang, J., Cheng, A. and Fang, X. [2018], Elastic reverse time migration using acoustic propagators. Geophysics, VOL. 83, NO. 5

Mao, J., Sheng, J., Huang, Y., Hao, F. and Liu, F. [2020], Multi-Channel dynamic matching full-waveform inversion, Extended Abstract, SEG 90th Annual meeting

Raknes, E., Arntsen, B. and Weibull, W. [2015], Three-dimensional elastic full waveform inversion using seismic data from the Sleipner area: *Geophysical Journal International*, 202.

Wang, B., He, Y., Mao, J., Liu, F., Hao, F., Huang, Y., Perz, M. and Michell, S. [2021], Inversion-based imaging: from LSRTM to FWI imaging: First Break, Vol. 39.

Wang, H., Burtz, O., Routh, P., Wang, D., Violet, J., Lu, R. and Lazaratos, S. [2021], Anisotropic 3D elastic full-wavefield inversion to directly estimate elastic properties and its role in interpretation: The Leading Edge.